Journal of Power Sources 222 (2013) 88–91

Contents lists available at SciVerse ScienceDirect

Journal of Power Sources

journal homepage: www.elsevier.com/locate/jpowsour

Short communication

Effects of CeO_2 on the microstructure and hydrogen evolution property of Ni–Zn coatings

Zhen Zheng [a], Ning Li [a,*], Chun-Qing Wang [b], De-Yu Li [a], Fan-Yu Meng [c], Yong-Ming Zhu [d]

[a] School of Chemical Engineering and Technology, Harbin Institute of Technology, Harbin 150001, China
[b] State Key Laboratory of Advanced Welding and Joining, Harbin Institute of Technology, Harbin 150001, China
[c] School of Municipal and Environmental Engineering, Harbin Institute of Technology, Harbin 150090, China
[d] Faculty of Applied Chemistry, Harbin Institute of Technology at Weihai, Weihai 264209, China

HIGHLIGHTS

- The correlation of synthesis–structure–activity is studied on Ni–Zn/CeO_2 coatings.
- The CeO_2 particles embedded in Ni–Zn matrix can increase the HER activity.
- A synergetic effect between CeO_2 particles and Ni–Zn matrix may exist in HER.
- The electrodes contained excess CeO_2 particles showed laminate morphology.

ARTICLE INFO

Article history:
Received 1 July 2012
Received in revised form
26 August 2012
Accepted 27 August 2012
Available online 3 September 2012

Keywords:
Nickel–zinc/ceria
Composite electrodes
Hydrogen evolution reaction
Deposition
Thin films

ABSTRACT

In this work, high-performance Ni–Zn/CeO_2 composite electrodes are prepared for hydrogen evolution reaction (HER) in alkaline solutions using a composite electrodeposition technique in a Ni–Zn bath containing suspended micro- or nano-sized CeO_2 particles. The composite electrodes containing more CeO_2 particles are dominant with laminate morphology. The addition of CeO_2 particles can alter the electrode phase composition. Optimization of the concentration of CeO_2 particles leads to a significant enhancement of HER activity on the composite electrodes, relative to Ni–Zn coating. The exchange current density of the composite electrode is 2 times higher than that of the Ni–Zn coating when the nano-CeO_2 concentration is 1 g L^{-1}. Electrochemical impedance spectroscopy results suggest that a possible synergetic effect on HER may exist between CeO_2 particles and Ni–Zn matrix.

1. Introduction

As a clean fuel, hydrogen has made a significant contribution in the solution of the energy crisis and greenhouse gas emission reduction [1,2]. In particular, the advanced water electrolysis technique is able to generate hydrogen efficiently, which prevents the use of the fossil fuels in the natural gas reforming or the gasification of coal and petroleum coke resulting in great environmental benefits. However, on current electrodes for water electrolysis, the high HER overpotential restrains hydrogen large scale application seriously [3]. In order to solve this problem, many novel electrode materials were synthesized to reduce both the HER overpotential and the cost [4,5]. Ni-based materials have attracted more and more attention due to their good activity for HER and sufficient corrosion resistance in the alkaline solution [6].

In principle, the activity for HER can be improved by increasing the real surface area and/or the intrinsic activity of the material [7]. Therefore, many Ni-based alloys have been studied on the HER activity, including Ni–Mo, Ni–S and Ni–Zn [8,9]. Based on Brewer–Engel theory, a synergistic effect [10] may exist between Ni and Mo; the Ni–S and Ni–Zn alloys exhibit a large real surface area [11,12]. Compared to the Ni-based alloys, Ni-based composite materials, such as Ni–MoO_x [13,14] and Ni-rare earth (RE) compounds [5] generally exhibited a higher activity for HER.

In this work, the Ni–Zn/CeO_2 composite electrodes were prepared by composite electrodeposition technique in a Ni–Zn bath containing CeO_2 particles. The CeO_2 particles incorporated in the Ni–Zn coating was found to affect the morphology and the

* Corresponding author. Tel.: +86 451 86413721; fax: +86 451 86418270.
E-mail address: lininghit@263.net (N. Li).

0378-7753/$ – see front matter © 2012 Elsevier B.V. All rights reserved.
http://dx.doi.org/10.1016/j.jpowsour.2012.08.077

preferred orientation of the coating. Two types of CeO_2 particle were chosen in this work: one is in micrometer scale, and the other is in nano-scale. The effects of both the CeO_2 particle size and concentration on the HER activity were systematically investigated.

2. Experimental

The Ni–Zn/CeO_2 composite electrodes were prepared on 10 × 10 cm^2 mild steel plates by composite electrodeposition technique from an electrolyte containing 120 g L^{-1} $NiCl_2$, 100 g L^{-1} $ZnCl_2$, 200 g L^{-1} KCl, 30 g L^{-1} H_3BO_3, 100 g L^{-1} ammonium acetate and either micro-CeO_2 (5–7 μm) or nano-CeO_2 (20–30 nm) particles. The composite electrodeposition was conducted at a current density of 3 A dm^{-2} for about 1 h at 313 K with a magnetic stirrer at 600 rpm. The obtained composite coatings with micro- or nano-sized CeO_2 were denoted as M-*n* or N-*n*, respectively (n = 1 and 2, when the concentration of CeO_2 particles was 1 g L^{-1} and 10 g L^{-1}).

The morphology and crystal structure of the composite coatings were determined by SEM (FEI Quanta 200F) and XRD (D/max-rB). The composition of the coating was analyzed by EDX coupled with SEM. Electrochemical tests were performed on a CHI 660 electrochemical workstation (CH Instrument, USA) using a standard three-electrode electrochemical cell. A Pt foil was used as the counter electrode and Hg/HgO/OH^- electrode (in 1.0 M NaOH) as the reference electrode at 298 K in 1.0 M NaOH solution. The EIS measurements were performed in the frequency region of 10 KHz–0.1 Hz with a voltage excitation amplitude of 5 mV at 298 K. The real (Z') and imaginary (Z'') components of electrochemical impedance spectra in the Nyquist plot were analyzed using the complex nonlinear least squares (CNLS) fitting program to simulate the equivalent resistances and capacitances.

3. Results and discussion

The morphology of the Ni–Zn and the CeO_2 incorporated composite electrodes are compared in Fig. 1. The microstructure of the Ni–Zn layer shows a typical flower shape. The microstructures of the M-1 and N-1 composite coatings are similar to that of the Ni–Zn coating, while finer and more compact morphology was observed in the N-1 composite coating relative to the Ni–Zn coating. This may indicate a larger surface area. According to Fig. 1c and e, the surface microstructures of the M-2 and N-2 composite coatings show laminate structure, which is obviously different with those of the Ni–Zn, M-1 and N-1 coatings. This may be attributable to the fact that excess CeO_2 particles were incorporated in the Ni–Zn coating and thus decreased the surface area. Based on the EDX analysis, the molar ratio of Ni-to-Zn is 86% in the Ni–Zn coating. The molar ratios of Ni-to-Zn in the M-1 and N-1 composite coatings are almost the same to that of the Ni–Zn coating, while the molar ratios of Ni-to-Zn in the M-2 and N-2 coatings are, 55% and 63%, respectively. They are much lower than the ratio of the Ni–Zn coating. The Ni–Zn codeposition process is an anomalous form. The addition of CeO_2 particles increases the Zn proportion in the composite coatings. As a result, this may be attributed to the formation acceleration of H_{ads} on CeO_2 particles, which is propitious to the crystallization of zinc [15].

According to the EDX results, it is found that the micro CeO_2 is easier to be co-deposited into the Ni–Zn layer relative to the nano-CeO_2. For example, the CeO_2 concentration in the M-2 coating is 18.9%, but the concentration in the N-2 coating is only 6.9%. These results are consistent with the reduction of particle size resulted from decreasing the co-deposition content of the CeO_2 particles [16].

Fig. 2 shows the phase composition and structure of the Ni–Zn coatings with and without CeO_2 particle incorporation. The Ni–Zn coating consists of $NiZn_3$ (JCPDF No. 47-1019), Ni_2Zn_{11} (JCPDF No. 65-5310) and $NiZn_{7.33}$ (JCPDF No. 65-9641) intermetallic compounds. When micro-CeO_2 particles are embedded in the coating, a new phase NiZn (JCPDF No. 65-9470) takes the place of Ni_2Zn_{11} in the M-2 composite coating. In the case of the nano-CeO_2 particle, the main phase composition found in composite coating is similar to that of the Ni–Zn coating, while the proportion of each phase is different to Ni–Zn alloy phases in the N-2 composite coating. It can be seen that both the structure and the preferred orientation of the Ni–Zn coating have been greatly changed, when the different sized CeO_2 particles are incorporated in the coatings. The existence or formation of different chemical species adsorbed at the metal–electrolyte interface can be affected due to the addition of the CeO_2 particles. The embedded CeO_2 particles can act as an acceptor for hydrogen adsorption [13]. As a result, they can influence the pH value near the cathode area, and then affect the concentration of intermediate such as $Zn(OH)_2$, $Ni(OH)_2$ and H_{ads}.

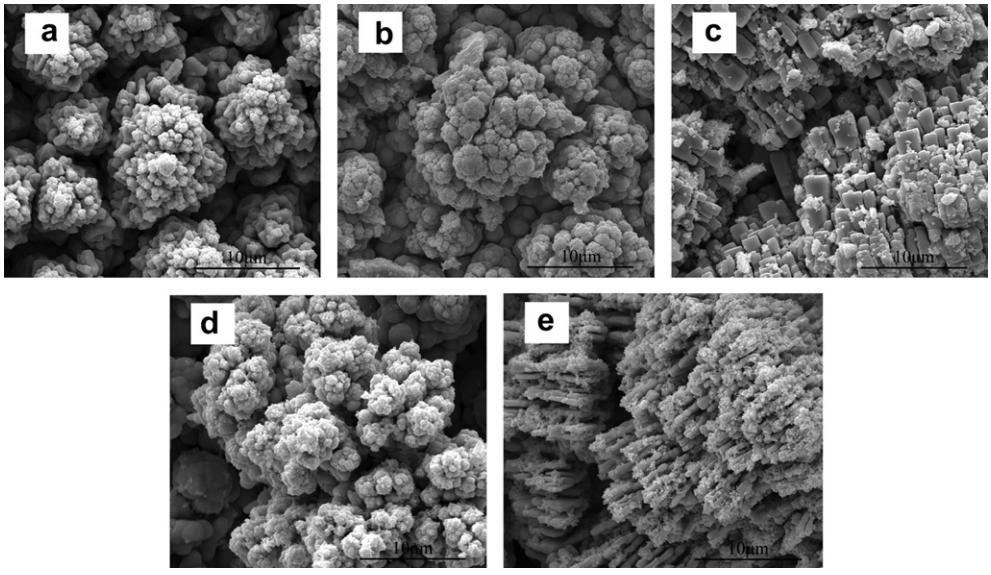

Fig. 1. SEM images of the Zn–Ni alloy and the Zn–Ni/CeO_2 composite coatings. (a) The Ni–Zn, (b) M-1, (c) M-2, (d) N-1, and (e) N-2 composite coatings.

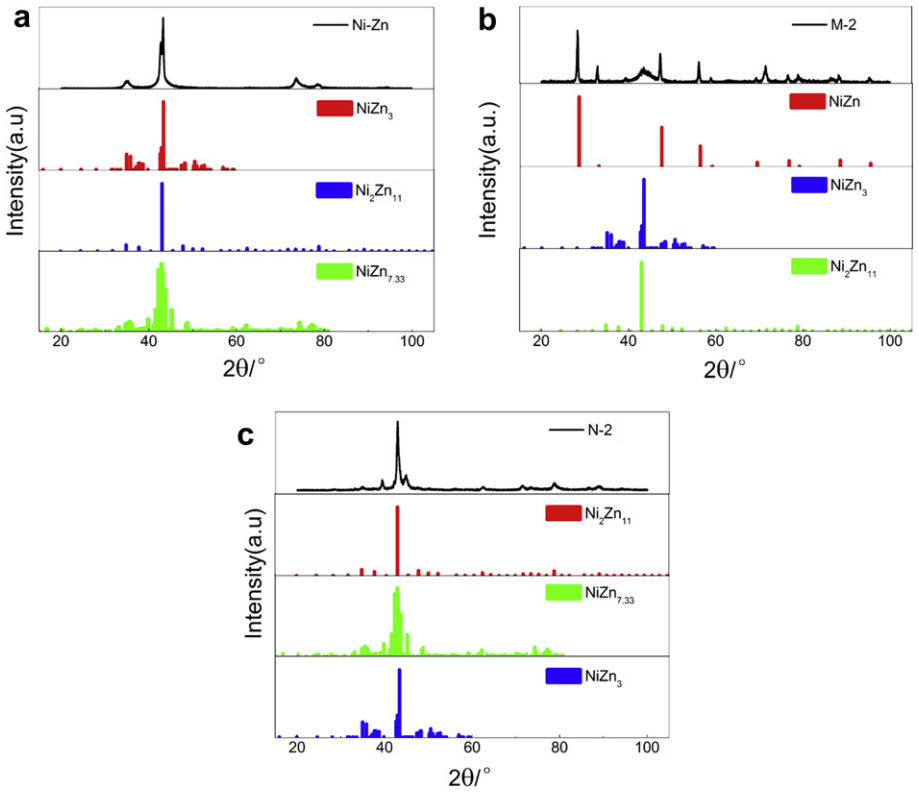

Fig. 2. XRD patterns of the Ni–Zn and Zn–Ni/CeO_2 composite coatings. (a) Zn–Ni layer, (b) M-2 composite coating, and (c) N-2 composite coating.

The steady-state linear polarization curves for HER recorded in 1.0 M NaOH at room temperature on the selected Ni–Zn, micro- and nano-CeO_2 composite electrodes are compared in Fig. 3. The curves display a typical Tafel region, and the Tafel equation can be written as following:

$$\eta_c = -\frac{2.3RT}{\alpha nF}\log j_0 + \frac{2.3RT}{\alpha nF}\log j \quad (1)$$

Here η_c is the cathode overpotential, R is the ideal gas constant, and T is the absolute temperature, α, n and F are the charge-transfer coefficient, number of electrons exchanged and the Faraday constant, respectively. And j_0 is the apparent exchange current density, which can represent the HER activity of the electrodes [17].

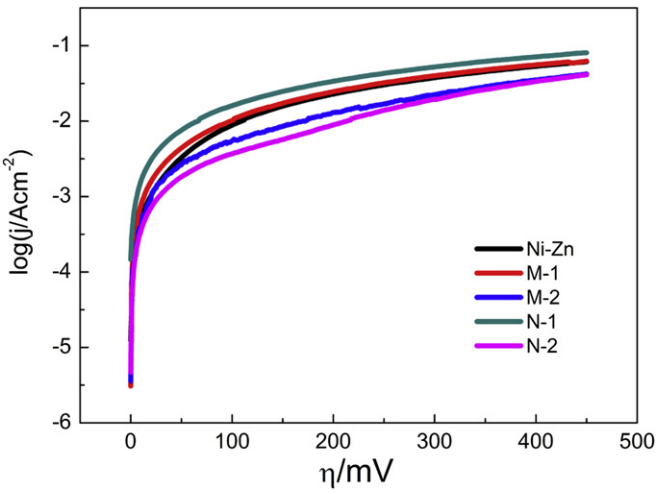

Fig. 3. Steady-state polarization curves of the HER on the Ni–Zn and Zn–Ni/CeO_2 composite coatings in 1.0 M NaOH solution at 298 K.

The calculated kinetic parameters of the Ni–Zn and composite electrodes are listed in Table 1. It can be seen that the j_0 values on the M-1 and N-1 composite electrodes are larger than that on the Ni–Zn coating, especially the j_0 value on the N-1 electrode is 2.2 times higher than that on the Ni–Zn coating, indicating that the M-1 and N-1 composite coatings have a high HER intrinsical activity. According to the SEM image of M-1 coating, the surface area of composite electrode slightly decreases with the addition of the micro-CeO_2 particles, and this can reduce the HER activity. Because the Ce atom contains half-filled and empty d orbitals, the reduction product, i.e. H atom can easily adsorb on Ce. Hence, a possible synergetic effect between CeO_2 and the Ni–Zn matrix can enhance the HER activity. The microstructure of the N-1 coating is finer with a larger surface area compared to Ni–Zn coating. Meanwhile, the synergetic effect also enhances the activity. The HER activity on the N-1 composite coating is much higher than that on the Ni–Zn coating. However, the HER activity are greatly reduced on the M-2 and N-2 coatings, when too much CeO_2 particles are embedded in the Ni–Zn coating. This may be due to that the microstructure and the phase composition will be greatly

Table 1
Electrocatalytic parameters of the HER obtained from the polarization curves recorded in 1 M NaOH solution at 298 K.

Electrode	b/mV dec^{-1}	j_0/mA cm^{-2}	α
Ni–Zn	119	2.47	0.49
M-1	140	2.74	0.41
N-1	146	5.37	0.40
M-2	150	1.86	0.39
N-2	168	1.49	0.35

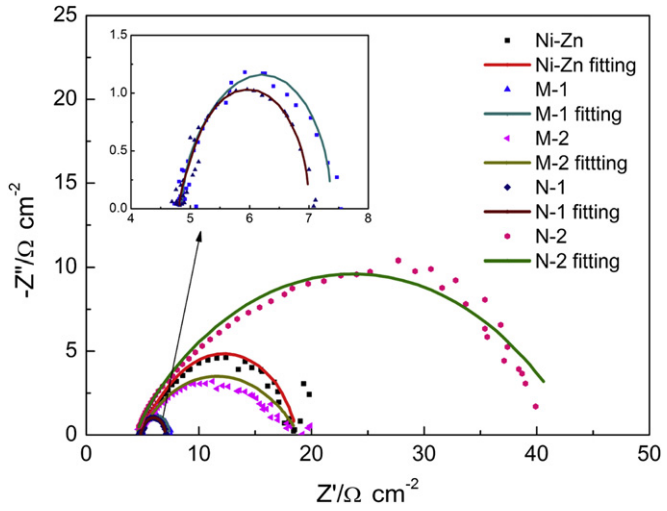

Fig. 4. Nyquist plots of for the HER on Ni–Zn, micro and nano-CeO_2 based composite electrodes at an overpotential of 50 mV in 1.0 M NaOH solution at 298 K. (Experimental (symbols) and fitted (solid lines))

changed. The laminate structure was found as a dominant factor in the reduction of the HER activity.

Tafel slope b is an important parameter and can provide insights into the HER mechanism on the composite electrodes. When CeO_2 particles embedded in the Ni–Zn coating, the composite electrodes showed a high Tafel slope value [17]. According to the Tafel equation, $b = 2.3RT/(\alpha F)$, the charge-transfer coefficient α related to the possible rate-determining step (RDS) can be calculated. As listed in Table 1, all if the α values are all less than 0.5, suggesting that the RDS of HER on the studied composite electrodes may be the Volmer reaction or the Volmer reaction coupled with Heyrovsky reaction or Tafel reaction [18].

In order to investigate the interfacial properties and electro-catalysis kinetics of the HER on Ni–Zn and the composite electrodes, impedance measurements were further carried out at a wide frequency range (10 KHz–0.1 Hz). The classic complex plane Nyquist plots were obtained on the composite electrodes and Ni–Zn electrodes at cathode overpotential of 50 mV, as shown in Fig. 4. The electrical circuit model selected to investigate the HER electrochemical process was shown in Fig. 5, which was similar to elsewhere proposed [19]. In the equivalent circuit, R_s is the solution resistance. R_{ct} is the electrochemical charge transfer resistance. CPE1 is associated with the double layer capacitance (C_{dl}). R_p is related to the resistance of the adsorbed intermediate H_{ads}, and CPE2 is the constant phase element of the pseudo-capacitance [20,21].

The values of the electrochemical parameters simulated from the analysis of impedance spectra are reported in Table 2. The

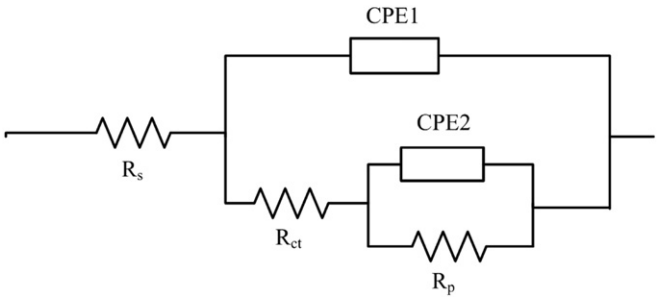

Fig. 5. Equivalent electric circuit used for fitting the EIS experimental results.

Table 2
Electrocatalysis parameters obtained from the EIS measurements.

Samples	Ni–Zn	M-1	M-2	N-1	N-2
$R_{ct}(\Omega\ cm^{-2})$	4.33	1.57	2.32	0.70	2.56
$R_p(\Omega\ cm^{-2})$	9.49	0.95	12.31	1.49	36.77

overall electrochemical reaction resistance values ($R_{ct} + R_p$) decreases obviously with the size of CeO_2 particles embedded in the Ni–Zn electrode. So the different sized CeO_2 particles may make the synergetic effect with the Ni–Zn matrix during the HER process, accelerate the formation of the H_{ads}. This experimental finding is consistent with our conclusion on the Ni–CeO_2 composite electrodes. When the excess micro or nano-sized CeO_2 particles embedded in the Ni–Zn coating (M-2 or N-2 composite electrodes), the overall electrochemical reaction resistance values ($R_{ct} + R_p$) increased. The decrease in the surface area and the influence in the H_{ads} desorption process can both decrease the HER activity of the M-2 and N-2 electrodes.

4. Conclusions

The Ni–Zn and Ni–Zn composite electrodes embedding micro- or nano-CeO_2 particles were prepared by the composite electrodeposition technique. The effects of the particle size and concentration of the CeO_2 particles on the morphology and crystalline structure of electrodes were systematically investigated. The morphology of the M-2 and N-2 coatings was characterized with laminate structure. The highest activity for the HER was achieved on the N-1 composite electrode containing an intermediate CeO_2 particle content. When excess CeO_2 particles were incorporated in the Ni–Zn coating, the decreased HER activity was observed.

References

[1] D.A. Dalla Corte, C. Torres, P.d.S. Correa, E.S. Rieder, C.d.F. Malfatti, International Journal of Hydrogen Energy 37 (2012) 3025–3032.
[2] W.E. Winsche, K.C. Hoffman, F.J. Salzano, Science 180 (1973) 1325–1332.
[3] R. Solmaz, A. Döner, G. Kardaş, Electrochemistry Communications 10 (2008) 1909–1911.
[4] K. Zeng, D. Zhang, Progress in Energy and Combustion Science 36 (2010) 307–326.
[5] D.E. Brown, M.N. Mahmood, A.K. Turner, S.M. Hall, P.O. Fogarty, International Journal of Hydrogen Energy 7 (1982) 405–410.
[6] M.A. Domínguez-Crespo, A.M. Torres-Huerta, B. Brachetti-Sibaja, A. Flores-Vela, International Journal of Hydrogen Energy 36 (2011) 135–151.
[7] I. Herraiz-Cardona, E. Ortega, J.G. Antón, V. Pérez-Herranz, International Journal of Hydrogen Energy 36 (2011) 9428–9438.
[8] I. Herraiz-Cardona, E. Ortega, V. Pérez-Herranz, Electrochimica Acta 56 (2011) 1308–1315.
[9] D.E. Brown, M.N. Mahmood, M.C.M. Man, A.K. Turner, Electrochimica Acta 29 (1984) 1551–1556.
[10] M.M. Jakšić, Electrochimica Acta 45 (2000) 4085–4099.
[11] I. Herraiz-Cardona, E. Ortega, L. Vázquez-Gómez, V. Pérez-Herranz, International Journal of Hydrogen Energy 36 (2011) 11578–11587.
[12] F. Rosalbino, D. Maccio, E. Angelini, A. Saccone, S. Delfino, International Journal of Hydrogen Energy 33 (2008) 2660–2667.
[13] N.V. Krstajić, L. Gajić-Krstajić, U. Lačnjevac, B.M. Jović, S. Mora, V.D. Jović, International Journal of Hydrogen Energy 36 (2011) 6441–6449.
[14] N.V. Krstajić, U. Lačnjevac, B.M. Jović, S. Mora, V.D. Jović, International Journal of Hydrogen Energy 36 (2011) 6450–6461.
[15] M. Eyraud, Z. Hanane, J. Crousier, Surface and Coatings Technology 67 (1994) 35–42.
[16] S.-C. Wang, W.-C.J. Wei, Materials Chemistry and Physics 78 (2003) 574–580.
[17] J. Kubisztal, A. Budniok, A. Lasia, International Journal of Hydrogen Energy 32 (2007) 1211–1218.
[18] J.M. Jakšić, M.V. Vojnović, N.V. Krstajić, Electrochimica Acta 45 (2000) 4151–4158.
[19] R.D. Armstrong, M. Henderson, Journal of Electroanalytical Chemistry and Interfacial Electrochemistry 39 (1972) 81–90.
[20] F. Rosalbino, S. Delsante, G. Borzone, E. Angelini, International Journal of Hydrogen Energy 33 (2008) 6696–6703.
[21] A. Damian, S. Omanovic, Journal of Power Sources 158 (2006) 464–476.